

**Structural differences in amyloid- β fibrils from brains of non-demented elderly individuals
and Alzheimer's disease patients**

Ujjayini Ghosh^{1,2}, Wai-Ming Yau¹, John Collinge³, and Robert Tycko^{1*}

¹Laboratory of Chemical Physics, National Institute of Diabetes and Digestive and Kidney Diseases, National Institutes of Health, Bethesda, MD 20892-0520, USA

²Department of Chemistry, Michigan State University, East Lansing, MI 48824, USA

³MRC Prion Unit and Institute of Prion Diseases, University College London, London W1W 7FF, UK

*corresponding author: Dr. Robert Tycko, National Institutes of Health, Building 5, Room 409, Bethesda, MD 20892-0520, USA. email: robertty@mail.nih.gov; phone: 301-402-8272

keywords: amyloid structure, Alzheimer's disease, solid state NMR

Abstract

Although amyloid plaques comprised of fibrillar amyloid- β ($A\beta$) assemblies are a diagnostic hallmark of Alzheimer's disease (AD), quantities of amyloid similar to those in AD patients are observed in brain tissue of some non-demented elderly individuals. The relationship between amyloid deposition and neurodegeneration in AD has therefore been unclear. Here we use solid state nuclear magnetic resonance (NMR) to investigate whether molecular structures of $A\beta$ fibrils from brain tissue of non-demented elderly individuals with high amyloid loads differ from structures of $A\beta$ fibrils from AD tissue. Two-dimensional solid state NMR spectra of isotopically labeled $A\beta$ fibrils, prepared by seeded growth from frontal lobe tissue extracts, are similar in the two cases, but with statistically significant differences in intensity distributions of crosspeak signals. Differences in solid state NMR data are greater for 42-residue ($A\beta_{42}$) fibrils than for 40-residue ($A\beta_{40}$) fibrils. These data suggest that similar sets of fibril polymorphs develop in non-demented elderly individuals and AD patients, but with different relative populations on average.

Significance statement

Alzheimer's disease (AD) patients develop amyloid deposits, containing amyloid- β ($A\beta$) fibrils, in their brain tissue. Although amyloid is a likely contributor to AD dementia, similar amyloid loads occur in some non-demented elderly individuals. Molecular structures of $A\beta$ fibrils are known to be variable. We therefore investigate whether structures of $A\beta$ fibrils derived from cerebral cortical tissue of non-demented elderly subjects differ from structures from AD patients. We find statistically significant, but subtle, differences between nuclear magnetic resonance (NMR) spectra of $A\beta$ fibrils from non-demented elderly subjects and analogous spectra of fibrils from AD patients. Thus, similar structures develop, but with different relative populations on average. Other factors may be primary determinants of cognitive status in individuals with high amyloid loads.

Amyloid plaques in brain tissue, containing fibrils formed by amyloid- β (A β) peptides, are one of the diagnostic pathological signatures of Alzheimer's disease (AD). Clear genetic and biomarker evidence indicates that A β is key to AD pathogenesis (1). However, A β is present as a diverse population of multimeric assemblies, ranging from soluble oligomers to insoluble fibrils and plaques, and may lead to neurodegeneration by a number of possible mechanisms (2-7).

One argument against a direct neurotoxic role for A β plaques and fibrils in AD is the fact that plaques are not uncommon in the brains of non-demented elderly people, as shown both by traditional neuropathological studies (8,9) and by positron emission tomography (10-13). On average, the quantity of amyloid is greater in AD patients (10) and (at least in some studies) increases with decreasing cognitive ability (12,14,15) or increasing rate of cognitive decline (16). However, a high amyloid load does not necessarily imply a high degree of neurodegeneration and cognitive impairment (11,13,17).

A possible counter-argument comes from studies of the molecular structures of A β fibrils, which show that A β peptides form multiple distinct fibril structures, called fibril polymorphs (18-20). Polymorphism has been demonstrated for fibrils formed by both 40-residue (19,21-24) and 42-residue (22,25-29) A β peptides (A β 40 and A β 42), the two main A β isoforms. Among people with similar total amyloid loads, variations in neurodegeneration and cognitive impairment may conceivably arise from variations in the relative populations of different fibril polymorphs. As a hypothetical example, if polymorph A was neurotoxic but polymorph B was not, then people whose A β peptides happened to form polymorph A would develop AD, while people whose A β peptides happened to form polymorph B would remain cognitively normal. In practice, brains may contain a population of different propagating and/or neurotoxic A β species, akin to prion quasispecies or "clouds", and the relative proportions of these and their dynamic interplay may affect clinical phenotype and rates of progression (30).

Well-established connections between molecular structural polymorphism and variations in other neurodegenerative diseases lend credence to the hypothesis that A β fibril polymorphism plays a role in variations in the characteristics of AD. Distinct strains of prions causing the transmissible spongiform encephalopathies have been shown to involve different molecular structural states of the mammalian prion protein PrP (30-32). Distinct tauopathies involve different polymorphs of tau protein fibrils (33-37). In the case of synucleopathies, α -synuclein

has been shown to be capable of forming polymorphic fibrils (38-40) with distinct biological effects (41-43).

Experimental support for connections between A β polymorphism and variations in characteristics of AD comes from polymorph-dependent fibril toxicities in neuronal cell cultures (19), differences in neuropathology induced in transgenic mice by injection of amyloid-containing extracts from different sources (44-46), differences in conformation and stability with respect to chemical denaturation of A β assemblies prepared from brain tissue of rapidly or slowly progressing AD patients (47), and differences in fluorescence emission spectra of structure-sensitive dyes bound to amyloid plaques in tissue from sporadic or familial AD patients (48,49).

Solid state nuclear magnetic resonance (NMR) spectroscopy is a powerful method for investigating fibril polymorphism because even small, localized changes in molecular conformation or structural environment produce measurable changes in ^{13}C and ^{15}N NMR chemical shifts, *i.e.*, in NMR frequencies of individual carbon and nitrogen sites. Full molecular structural models for amyloid fibrils can be developed from large sets of measurements on structurally homogeneous samples (21,25,26,29,38,50). Alternatively, simple two-dimensional (2D) solid state NMR spectra can serve as structural fingerprints, allowing assessments of polymorphism and comparisons between samples from different sources (22,51).

Solid state NMR requires isotopic labeling and milligram-scale quantities of fibrils, ruling out direct measurements on amyloid fibrils extracted from brain tissue. However, A β fibril structures from autopsied brain tissue can be amplified and isotopically labeled by seeded fibril growth, in which fibril fragments (*i.e.*, seeds) in a brain tissue extract are added to a solution of isotopically labeled peptide (21,22,52). Labeled "daughter" fibrils that grow from the seeds retain the molecular structures of the "parent" fibrils, as demonstrated for A β (19,21,24,53) and other (54,55) amyloid fibrils. Solid state NMR measurements on the brain-seeded fibrils then provide information about molecular structures of fibrils that were present in the brain tissue at the time of autopsy. Using this approach, Lu *et al.* developed a full molecular structure for A β 40 fibrils derived from one AD patient with an atypical clinical history (patient 1), showed that A β 40 fibrils from a second patient with a typical AD history (patient 2) were qualitatively different in structure, and showed that the predominant brain-derived A β 40 polymorph was the same in multiple regions of the cerebral cortex from each patient (21). Subsequently, Qiang *et al.* prepared isotopically labeled A β 40 and A β 42 fibrils from frontal, occipital, and parietal lobe tissue of 15 patients in

three categories, namely typical long-duration AD (t-AD), the posterior cortical atrophy variant of AD (PCA-AD), and rapidly progressing AD (r-AD) (22). Quantitative analyses of 2D solid state NMR spectra led to the conclusions that A β 40 fibrils derived from t-AD and PCA-AD tissue were indistinguishable, with both showing the same predominant polymorph, that A β 40 fibrils derived from r-AD tissue were more structurally heterogeneous (*i.e.*, more polymorphic), and that A β 42 fibrils derived from all three categories were structurally heterogeneous, with at least two prevalent A β 42 polymorphs (22).

In this paper, we address the question of whether A β fibrils that develop in cortical tissue of non-demented elderly individuals with high amyloid loads are structurally distinguishable from fibrils that develop in cortical tissue of AD patients. As described below, quantitative analyses of 2D solid state NMR spectra of brain-seeded samples indicate statistically significant differences for both A β 40 and A β 42 fibrils. Differences in the 2D spectra are subtle, however, indicating that non-demented individuals and AD patients do not develop entirely different A β fibril structures. Instead, data and analyses described below suggest overlapping distributions of fibril polymorphs, with different relative populations on average.

Results

Preparation of A β fibrils

A β 40 and A β 42 fibrils were prepared by seeded growth, using an amyloid-containing extract from human frontal lobe tissue as the source of seeds. As in the experiments of Qiang *et al.* (22), A β 40 was ^{15}N , ^{13}C -labeled at F19, V24, G25, S26, A30, I31, L34, and M35, and A β 42 was ^{15}N , ^{13}C -labeled at F19, G25, A30, I31, L34, and M35. Tissue samples were obtained from the Religious Orders Study (ROS) of the Rush Alzheimer's Disease Center (RADC) (56). Eight samples were selected from subjects assessed as lacking cognitive impairment but with high cortical A β levels measured by immunohistochemistry (see SI Methods section and Table S1 of the SI Appendix). Ages at death ranged from 85 to 100 years.

Extracts were prepared as described previously (21,22). Fibrils were then grown with the protocol depicted in Fig. 1a. This protocol is identical to the one used by Qiang *et al.*, except that isotopically labeled A β , solubilized in dimethyl sulfoxide (DMSO), was added to the sonicated suspension of tissue extract in two steps rather than in a single step (SI Appendix, SI Methods).

This modification of the seeded growth protocol was necessary because tissue samples from RADC were only 0.5-0.6 g, whereas tissue samples in the experiments of Qiang *et al.* were approximately 2.0-3.0 g. By adding A β in two steps, the ratio of DMSO-solubilized A β to extract at the beginning of fibril growth was kept approximately constant. To minimize the likelihood of preferential amplification of specific polymorphs (57), sonication conditions that fragment all polymorphs were used, multiple rounds of seeded growth were avoided, and the ratio of A β in seeds to soluble A β in the second step was large (2:13 ratio).

Fibril samples derived from RADC tissue are denoted RADC n f, with $n = 1, 2, \dots, 8$ and with "f" indicating frontal lobe tissue. Figs. 1b and 1c show examples of TEM images of A β 40 and A β 42 fibrils after the initial 4 h growth period and after the subsequent 18-24 h period. Full sets of TEM images are shown in Figs. S1 and S2 of the SI Appendix. The TEM images at 4 h show fibrils in all cases, whereas previously reported control experiments with extracts from human cortical tissue that was devoid of A β plaques resulted in no detectable fibrils after 4 h (21,22). The morphologies of A β 40 and A β 42 fibrils in the TEM images could not be assessed reliably because, in many cases, extraneous material from the tissue extracts adhered to or partially obscured the fibrils. It should be noted that our tissue extracts are heterogeneous materials, with amyloid representing only a small fraction of the total mass.

Solid state NMR spectroscopy of A β 40 fibrils

Figs. 2a and 2b show examples of 2D ^{13}C - ^{13}C solid state NMR spectra of A β 40 fibrils prepared by seeded growth from RADC tissue extracts. The 2D spectrum in Fig. 2a exhibits a single set of relatively sharp and strong crosspeaks, with little intensity in additional signals. This spectrum therefore suggests a single predominant A β 40 fibril polymorph in the RADC1f sample. Additional signals in Fig. 2b, indicated by cyan arrows, suggest the presence of at least one additional polymorph with substantial population in the RADC4f sample. One-dimensional (1D) spectra of all eight RADC A β 40 samples (Figs. S3a and S3c, SI Appendix) show variations in the relative intensities and shapes of the ^{13}C solid state NMR lines, suggesting variations in polymorph populations. The full set of 2D ^{13}C - ^{13}C spectra is shown in Fig. S4 of the SI Appendix.

For comparison, Figs. 2c and 2d show 2D ^{13}C - ^{13}C solid state NMR spectra of A β 40 fibrils prepared by seeded growth from one of the typical long-duration AD tissue extracts examined by

Qiang *et al.* (22) (sample t-AD4f) and A β 40 fibrils prepared *in vitro* without seeding. Spectra in Figs. 2b and 2c are similar to one another, whereas the spectrum in Fig. 2d shows broader crosspeaks and additional signals, indicating greater structural heterogeneity in the final fibril sample when fibril growth is initiated by spontaneous nucleation, rather than by seeding.

Figs. 2e-h shows 2D ^{15}N - ^{13}C solid state NMR spectra of the same A β 40 fibrils as in Figs. 2a-d. Again, the spectrum of the RADC4f sample (Fig. 2f) shows additional crosspeak signals that are not detectable in the spectrum of the RADC1f sample (Fig. 2e). The spectrum of the t-AD4f sample (Fig. 2g) is similar to that of the RADC4f sample, but differences are more readily apparent than in the 2D ^{13}C - ^{13}C spectra. The 2D ^{15}N - ^{13}C spectrum of the unseeded sample (Fig. 2h) obviously contains many crosspeak signals that are not present in spectra of the other three samples. 2D ^{15}N - ^{13}C spectra of all eight RADC A β 40 samples are shown in Fig. S5 of the SI Appendix.

Solid state NMR spectroscopy of A β 42 fibrils

Fig. 3 shows 2D ^{13}C - ^{13}C and ^{15}N - ^{13}C solid state NMR spectra of RADC3f and RADC7f A β 42 fibrils, t-AD1f A β 42 fibrils from the work of Qiang *et al.* (22), and unseeded A β 42 fibrils. 2D spectra of all eight RADC A β 42 fibrils are shown in Figs. S6 and S7 of the SI Appendix. Both types of 2D spectra show clear differences between the RADC3f and RADC7f samples, suggesting that the main A β 42 fibril polymorphs in these two samples are different. 2D spectra of t-AD1f A β 42 fibrils are also different from the two RADC samples. 2D spectra of the unseeded A β 42 fibrils contain broader crosspeaks and additional crosspeaks, indicating greater structural heterogeneity.

As with the A β 40 fibrils, 1D spectra of all eight RADC A β 42 samples (SI Appendix, Figs. S3b and S3d) show variations in the relative intensities and shapes of the ^{13}C solid state NMR lines. These spectra also show large variations in total signal amplitude (*e.g.*, a factor of four difference between RADC4f and RADC8f A β 42 samples, see Fig. S3d of the SI Appendix), although the amount of isotopically labeled A β 42 used in the seeded fibril growth protocol was the same for each sample. Variations in signal amplitude are attributable to variations in the quantities of seed-competent A β 42 amyloid in the tissue samples. In particular, signals from the RADC2f A β 42 sample were very weak, leading to barely detectable crosspeaks in 2D spectra of

this sample (SI Appendix, Figs. S6 and S7).

RMSD analyses

If the brain-seeded A β 40 and A β 42 fibril samples contained only a small number of polymorphs and if their crosspeak signals were well resolved in the 2D spectra, then it would be possible to estimate the populations of individual polymorphs in each sample from crosspeak volumes in the 2D spectra. In reality, however, the 2D spectra contain complicated crosspeak patterns, with contributions from multiple polymorphs that are not well resolved. Therefore, we used two objective methods for quantitatively analyzing and comparing 2D spectra that do not require assignment of crosspeaks to individual polymorphs.

In the first method, we calculated pairwise root-mean-squared differences (RMSDs) among signal amplitudes in the 2D spectra, after identifying regions of the spectra that contain signals above the noise level, normalizing the total signal amplitudes, and optimizing the relative scaling of signal amplitudes (see SI Methods section of the SI Appendix). Fig. 4 displays pairwise RMSDs among 2D solid state NMR spectra of A β 40 and A β 42 fibrils as heat maps, with small RMSD values in blue, intermediate values in white and yellow, and large values in red. 2D spectra of the eight RADC-seeded samples are included, along with 2D spectra of t-AD and PCA-AD samples reported previously by Qiang *et al.* (22). (2D spectra of all t-AD and PCA-AD samples appear in Extended Data Figs. 2 and 3 of the paper by Qiang *et al.* and are available at <https://doi.org/10.17632/tbp45pm92x.1> .) Fibrils derived by seeded growth from amyloid-containing extracts of t-AD and PCA-AD tissue samples are denoted by t-AD $_n$ x and PCA $_n$ x, where n is the patient number and x is "f", "o", or "p" for frontal, occipital, or parietal lobe tissue, respectively. Although RMSD values vary considerably when spectra within or between each of the three tissue categories (*i.e.*, RADC, t-AD, and PCA-AD) are compared, the overall color patterns in all four panels of Fig. 4 suggest that 2D spectra of RADC samples are more similar to one another (*i.e.*, have smaller pairwise RMSDs on average) than to 2D spectra of t-AD or PCA-AD samples. Moreover, as shown previously by Qiang *et al.* (22), t-AD and PCA-AD samples appear to be indistinguishable. The sensitivity of RMSD values to differences among 2D spectra is evident, for example, from the observation that 2D ^{13}C - ^{13}C spectra of RADC1f and t-AD4f fibrils appear similar in the contour plots in Fig. 2 but have RMSD = 0.28, while 2D ^{13}C - ^{13}C spectra of RADC6f and RADC7f are more nearly identical in Fig. S4 of the SI Appendix and have RMSD

= 0.08.

Three statistical tests were used to evaluate the significance of the apparent differences in RMSD values. Results are summarized in Table 1. 2D spectra of RADC2f A β 42 were not included in these tests, due to their low signal-to-noise ratios.

First, the two-sample Kolmogorov-Smirnov (KS) test was used to determine whether distributions of RMSD values for pairs of spectra of RADC samples were significantly different from distributions of RMSD values between spectra of RADC samples and spectra of t-AD samples, PCA-AD samples, and combined t-AD and PCA-AD samples. Significant differences (*i.e.*, D statistic greater than critical value, with significance parameter $\alpha = 0.05$) were found in nearly all cases, for both A β 40 and A β 42 fibrils and for both 2D ^{13}C - ^{13}C spectra and 2D ^{15}N - ^{13}C spectra. The only exceptions were when RMSDs between 2D spectra of pairs of RADC A β 42 samples were compared with RMSDs between spectra of RADC A β 42 samples and spectra of PCA-AD A β 42 samples. The absence of statistical significance in these cases may be due to the small number of PCA-AD A β 42 samples for which 2D spectra were available.

Next, the two-tail, two-sample Wilcoxon-Mann-Whitney (WMW) test was used to confirm the KS results. The WMW test indicated significant differences between distributions of RMSD values ($p \leq 0.002$) in all cases where differences were significant according to the KS test.

Finally, Welch's t-test (WTT) was used to determine the statistical significance of differences between the average RMSD value for pairs of spectra of RADC samples and the average RMSD value between spectra of RADC samples and spectra of t-AD samples, PCA-AD samples, and combined t-AD and PCA-AD samples. Again, differences were found to be significant ($p \leq 0.002$) in all cases except when RMSDs between 2D spectra of pairs of RADC A β 42 samples were compared with RMSDs between spectra of RADC A β 42 samples and spectra of PCA-AD A β 42 samples.

In addition to the unseeded *in vitro* fibrils whose spectra are shown in Figs. 2d, 2h, 3d, and 3h, A β 40 and A β 42 fibrils were grown in the presence of extract from occipital lobe tissue that was devoid of detectable amyloid (22). Fig. S8 of the SI Appendix shows 2D spectra of these fibrils, along with their RMSDs relative to the 2D spectra of RADC, t-AD, and PCA-AD fibril samples. In most cases, RMSD values in Fig. S8 are greater than the values in Table 1. Thus, we have no evidence that non-amyloid components of cortical tissue extracts promote the formation

of the specific fibril polymorphs that we observe in fibrils created by seeding with amyloid-containing extracts.

Principal component analyses

As a second method of assessing similarities and differences among samples, we used principal component analysis (49,58,59). As applied to 2D solid state NMR spectra (22), principal component analysis is a mathematical procedure for representing each experimental 2D spectrum $E_k(v_1, v_2)$ as a linear combination of principal component spectra $P_q(v_1, v_2)$, with principal values η_q and coefficients c_{kq} , *i.e.*, $E_k(v_1, v_2) = \sum_{q=1}^N c_{kq} \eta_q P_q(v_1, v_2)$, where N is the number of experimental 2D spectra and v_1 and v_2 are the two frequency axes of the 2D spectra. Principal values are non-negative, and principal component spectra are ordered by decreasing principal value, *i.e.*, $\eta_q \geq \eta_{q'}$ if $q < q'$. The first principal component $P_1(v_1, v_2)$ is an approximate average of the experimental 2D spectra. Subsequent principal components represent variations among the experimental 2D spectra with decreasing importance.

Principal component analyses were carried out as described in the SI Methods section of the SI Appendix, including spectra of RADC, t-AD, and PCA-AD samples. The total number of 2D spectra was $N = 28$ for 2D ^{13}C - ^{13}C spectra of A β 40 fibrils, $N = 25$ for 2D ^{15}N - ^{13}C spectra of A β 40 fibrils, $N = 22$ for 2D ^{13}C - ^{13}C spectra of A β 42 fibrils, and $N = 19$ for 2D ^{15}N - ^{13}C spectra of A β 42 fibrils. The first three principal component spectra for each set of 2D spectra are plotted in Figs. S9 and S10 of the SI Appendix. Principal values are plotted in Fig. S11 of the SI Appendix.

Values of the coefficients c_{k1} , c_{k2} , and c_{k3} from principal component analyses of the four sets of 2D spectra are plotted in Fig. 5. As expected, average values of c_{k1} are nearly equal for RADC, t-AD, and PCA-AD samples. Average values of c_{k2} and c_{k3} vary, suggesting differences among 2D spectra from the three tissue categories. As for the RMSD analyses, three statistical tests were used to evaluate significance. Results are summarized in Table 2.

The KS test indicates that the distribution of c_{2k} values for 2D ^{13}C - ^{13}C spectra of RADC A β 40 fibrils differs significantly ($\alpha = 0.5$) from distributions of c_{2k} values for 2D ^{13}C - ^{13}C spectra of t-AD A β 40 fibrils, PCA-AD A β 40 fibrils, and combined t-AD and PCA-AD A β 40 fibrils. The

same is true for 2D ^{13}C - ^{13}C spectra of A β 42 fibrils. The KS test also indicates significant differences between the distribution of c_{2k} values for 2D ^{15}N - ^{13}C spectra of RADC A β 42 fibrils and distributions of c_{2k} values for 2D ^{15}N - ^{13}C spectra of t-AD A β 42 fibrils and combined t-AD and PCA-AD A β 42 fibrils, as well as significant differences between the distribution of c_{1k} values for 2D ^{13}C - ^{13}C spectra of RADC A β 42 fibrils and distributions of c_{1k} values for 2D ^{13}C - ^{13}C spectra of t-AD A β 42 fibrils and combined t-AD and PCA-AD A β 42 fibrils.

The WMW test indicates significant differences ($p \leq 0.005$) in all cases where differences were significant according to the KS test. Additionally, the WMW test indicates significant differences ($p \leq 0.029$) between the distribution of c_{2k} values for 2D ^{15}N - ^{13}C spectra of RADC A β 40 fibrils and distributions of c_{2k} values for 2D ^{15}N - ^{13}C spectra of t-AD A β 40 fibrils and combined t-AD and PCA-AD A β 42 fibrils, as well as a significant difference ($p = 0.034$) between the distribution of c_{1k} values for 2D ^{13}C - ^{13}C spectra of RADC A β 42 fibrils and the distribution of c_{1k} values for 2D ^{13}C - ^{13}C spectra of PCA-AD A β 42 fibrils.

Finally, for both A β 40 and A β 42 fibrils and for both 2D ^{13}C - ^{13}C spectra and 2D ^{15}N - ^{13}C spectra, WTT indicates significant differences ($p \leq 0.029$) between average values of c_{2k} for RADC samples and average values of c_{2k} for t-AD samples, PCA-AD samples, and combined t-AD and PCA-AD samples, except when 2D ^{15}N - ^{13}C spectra of RADC A β 42 samples are compared with 2D ^{15}N - ^{13}C spectra of PCA-AD A β 42 samples. WTT also indicates significant differences ($p \leq 0.040$) between the average value of c_{1k} for 2D ^{13}C - ^{13}C spectra of RADC A β 42 fibrils and the average values of c_{1k} for 2D ^{13}C - ^{13}C spectra of t-AD A β 42 fibrils, PCA-AD A β 42 fibrils, and combined t-AD and PCA-AD A β 42 fibrils.

Discussion

How do A β fibrils from non-demented subjects differ from A β fibrils from AD patients?

As described above, we have prepared isotopically labeled A β 40 and A β 42 fibrils by seeded growth from amyloid-containing extracts of cortical tissue from non-demented subjects with high amyloid loads (RADC samples), carried out solid state NMR measurements on these fibrils, and compared the resulting 2D solid state NMR spectra with previously reported (22) 2D spectra of isotopically labeled A β 40 and A β 42 fibrils derived from cortical tissue of AD patients (t-AD and PCA-AD samples). Both RMSD and principal component analyses indicate statistically

significant differences between spectra from RADC samples and spectra from t-AD and PCA-AD samples.

However, the differences are subtle. The 2D spectra are variable, both for fibrils derived from tissue of non-demented subjects (Figs. 2 and 3, Figs. S4-S7 of the SI Appendix) and for fibrils derived from tissue of AD patients (22). For example, 2D spectra of RADC1f A β 40 fibrils show a single set of strong crosspeak signals, indicating a single predominant structure and minimal polymorphism, while spectra of RADC3f A β 40 fibrils show multiple sets of signals, indicating a greater degree of polymorphism. Roughly speaking, 2D spectra of other RADC A β 40 fibrils are intermediate between those of RADC1f and RADC3f.

As a means of visualizing the differences between typical 2D spectra of fibrils derived from the three tissue categories, we constructed 2D spectra from the first three principal components (SI Appendix, Figs. S9 and S10), using the average values of c_{1k} , c_{2k} , and c_{3k} for each category. The resulting "average 2D spectra" are shown in Figs. 6 and 7. For A β 40 fibrils (Fig. 6), average 2D ^{13}C - ^{13}C and ^{15}N - ^{13}C spectra of RADC samples are similar to the corresponding average spectra of t-AD and PCA-AD spectra (which are essentially indistinguishable from one another). Differences in the relative intensities of crosspeak components arising from F19, V24, G25, and S26 are indicated by magenta arrows. For S26 and V24, the positions of maximal crosspeak intensity are shifted in the average 2D ^{13}C - ^{13}C spectra of t-AD and PCA-AD samples, relative to the positions of maximal crosspeak intensity in the average 2D ^{13}C - ^{13}C spectra of RADC samples.

For A β 42 (Fig. 7), differences between average 2D spectra of RADC samples and average 2D spectra of t-AD and PCA-AD samples are more pronounced. The most obvious differences are in the relative intensities of crosspeak components arising from F19, G25, A30, and I31. For G25, A30, and I31, positions of maximal crosspeak intensity are shifted in average 2D ^{13}C - ^{13}C or ^{15}N - ^{13}C spectra of t-AD and PCA-AD samples, relative to corresponding positions of maximal crosspeak intensity in average 2D spectra of RADC samples.

Thus, from the average 2D spectra, it appears that both non-demented subjects and AD patients develop distributions of A β 40 and A β 42 polymorphs in their cortical tissue. The distributions for non-demented subjects and AD patients overlap but exhibit statistically significant differences. The most obvious differences in the average 2D spectra are in crosspeak signals arising from G25, A30, and I31 in brain-seeded A β 42 fibrils. Other isotopically labeled residues in both A β 40 and A β 42 fibrils also exhibit significant differences in their average crosspeak

intensity distributions.

A β 40 versus A β 42

Our finding of greater differences on average for A β 42 fibrils suggests that the distribution of A β 42 fibril polymorphs in cortical tissue may be more predictive of cognitive impairment than the distribution of A β 40 fibril polymorphs. It should be recognized that cross-seeding between different A β isoforms, as observed *in vitro* under certain circumstances (60), may affect this finding. If cross-seeding is significant, solid state NMR data for A β 42 may not reflect only the properties of A β 42 fibrils in the original tissue. Nonetheless, it seems unlikely that seeding of A β 42 by A β 40 fibrils in our tissue extracts would produce greater structural variations among brain-seeded A β 42 fibrils than among brain-seeded A β 40 fibrils. Moreover, even if the molecular structures and structural distributions of brain-seeded fibrils in our experiments do not precisely match those of fibrils in the original cortical tissue, the fact that we see differences in solid state NMR spectra of fibrils derived from different groups of tissue samples supports the existence of structural differences in the original fibrils.

Implications for the role of A β fibril polymorphism in AD

Work described above was motivated by the goal of determining whether A β fibrils that develop in brain tissue of non-demented elderly subjects are structurally distinct from those that develop in brain tissue of AD patients. If clear differences in fibril structure exist, it would provide a potential explanation for the observation of high amyloid loads in some elderly individuals who are cognitively normal according to standard assessments (11,13,17). Our finding that 2D solid state NMR spectra of fibrils derived from cortical tissue of non-demented elderly individuals exhibit statistically significant differences from, but are nonetheless similar to, spectra of fibrils derived from cortical tissue of AD patients is best explained by the occurrence of the same or similar sets of fibril polymorphs in both cases, but with differences in the relative populations of these polymorphs on average. It is conceivable that certain polymorphs with enhanced populations in AD patients contribute most strongly to neurodegeneration. On the other hand, our data certainly do not rule out the possibility that factors other than A β fibril polymorphism are the primary determinants of cognitive status in subjects with high amyloid loads.

It has been proposed that cognitively normal subjects with high amyloid loads are in a preclinical phase of AD, meaning that they would eventually develop dementia (61). The absence of detectable cognitive impairment may be a consequence of large cognitive reserve in these individuals (62) and/or differential susceptibility to A β -induced neurotoxicity via variation in A β receptors (7). If neurodegeneration is driven largely by tau pathology that develops as a consequence of amyloid deposition (63), then variations in the strength of the A β -tau connection or susceptibility to tau-induced dysfunction could explain variations in cognitive impairment among individuals with high amyloid loads. The differences in relative populations of A β fibril polymorphs indicated by the solid state NMR data could then conceivably be a consequence of feedback, in which a neurodegenerative state, originally induced by amyloid formation, later alters the rates of clearance and self-propagation of certain A β fibril polymorphs. In this scenario, development of AD in some individuals with high amyloid loads, but not in others, would not be determined by differences in their A β fibril structures. However, once neurodegeneration became more pronounced in some individuals, the relative populations of various polymorphs in brain tissue of those with or without obvious cognitive impairment could become different on average.

Methods

Full details of samples, experiments, and data analyses are given in the SI Methods section of the SI Appendix.

Data and code availability

2D solid state NMR data that support the findings of this study are available at <https://doi.org/10.17632/dj34fwjhkt.1>. Computer programs written specifically for the analyses in Figs. 4 and 5 are available at <https://doi.org/10.17632/3ztc2dhx26.1>.

Author contributions

U.G., R.T., and J.C. designed the study. W.M.Y. synthesized and purified isotopically labeled A β peptides. U.G. and R.T. grew fibrils, acquired TEM and solid state NMR data, and analyzed the data. U.G., R.T., J.C., and W.M.Y. wrote the manuscript.

Conflicts of interest

The authors declare no conflicts of interest.

Acknowledgements

This work was supported by the Intramural Research Program of the National Institute of Diabetes and Digestive and Kidney Diseases, National Institutes of Health. The MRC Prion Unit at UCL is funded by the UK Medical Research Council and the National Institute of Health Research (NIHR) UCLH/UCL Biomedical Research Centre. We are grateful for the assistance of S. Mead, O. Avwenagha, and J. Wadsworth at the MRC Prion Unit in selection and processing of AD tissue samples. We thank the Queen Square Brain Bank for Neurological Disorders (supported by the Reta Lila Weston Trust for Medical Research, the Progressive Supranuclear Palsy [Europe] Association and the Medical Research Council) at the UCL Institute of Neurology, for provision of AD tissue samples. We thank all patients and their families for consent to use tissues in research. We thank Drs. David Bennett and Zoe Arvanitakis of RADc for providing tissue samples, with support from NIH grants P30AG010161 and R01AG15819. ROS data and resources can be requested at <https://www.radc.rush.edu>.

References

1. Selkoe, D.J. and Hardy, J., The amyloid hypothesis of Alzheimer's disease at 25 years. *EMBO Mol. Med.* **8**, 595-608 (2016).
2. Deane, R. and Zlokovic, B.V., Role of the blood-brain barrier in the pathogenesis of Alzheimer's disease. *Curr. Alzheimer Res.* **4**, 191-197 (2007).
3. Eikelenboom, P., *et al.*, Neuroinflammation - an early event in both the history and pathogenesis of Alzheimer's disease. *Neurodegener. Dis.* **7**, 38-41 (2010).
4. Jarosz-Griffiths, H.H., Noble, E., Rushworth, J.V., and Hooper, N.M., Amyloid- β receptors: The good, the bad, and the prion protein. *J. Biol. Chem.* **291**, 3174-3183 (2016).
5. Pithadia, A.S. and Lim, M.H., Metal-associated amyloid- β species in Alzheimer's disease. *Curr. Opin. Chem. Biol.* **16**, 67-73 (2012).
6. Delgado, D.A., *et al.*, Distinct membrane disruption pathways are induced by 40-residue β -amyloid peptides. *J. Biol. Chem.* **291**, 12233-12244 (2016).
7. Purro, S.A., Nicoll, A.J., and Collinge, J., Prion protein as a toxic acceptor of amyloid- β oligomers. *Biol. Psychiatry* **83**, 358-368 (2018).
8. Giannakopoulos, P., Hof, P.R., Michel, J.P., Guimon, J., and Bouras, C., Cerebral cortex

- pathology in aging and Alzheimer's disease: A quantitative survey of large hospital-based geriatric and psychiatric cohorts. *Brain Res. Rev.* **25**, 217-245 (1997).
9. Savva, G.M., *et al.*, Age, neuropathology, and dementia. *N. Engl. J. Med.* **360**, 2302-2309 (2009).
 10. Aizenstein, H.J., *et al.*, Frequent amyloid deposition without significant cognitive impairment among the elderly. *Arch. Neurol.* **65**, 1509-1517 (2008).
 11. Mathis, C.A., *et al.*, In vivo assessment of amyloid- β deposition in nondemented very elderly subjects. *Ann. Neurol.* **73**, 751-761 (2013).
 12. Grothe, M.J., *et al.*, Basal forebrain atrophy and cortical amyloid deposition in nondemented elderly subjects. *Alzheimers. Dement.* **10**, S344-S353 (2014).
 13. Gu, Y., *et al.*, Brain amyloid deposition and longitudinal cognitive decline in nondemented older subjects: Results from a multi-ethnic population. *PLoS One* **10**, (2015).
 14. Cummings, B.J., Pike, C.J., Shankle, R., and Cotman, C.W., β -Amyloid deposition and other measures of neuropathology predict cognitive status in Alzheimer's disease. *Neurobiol. Aging* **17**, 921-933 (1996).
 15. Naslund, J., *et al.*, Correlation between elevated levels of amyloid β -peptide in the brain and cognitive decline. *JAMA-J. Am. Med. Assoc.* **283**, 1571-1577 (2000).
 16. Villemagne, V.L., *et al.*, A β deposits in older non-demented individuals with cognitive decline are indicative of preclinical Alzheimer's disease. *Neuropsychologia* **46**, 1688-1697 (2008).
 17. Jack, C.R., *et al.*, Serial PIB and MRI in normal, mild cognitive impairment and Alzheimers disease: Implications for sequence of pathological events in Alzheimers disease. *Brain* **132**, 1355-1365 (2009).
 18. Goldsbury, C., Frey, P., Olivieri, V., Aebi, U., and Muller, S.A., Multiple assembly pathways underlie amyloid- β fibril polymorphisms. *J. Mol. Biol.* **352**, 282-298 (2005).
 19. Petkova, A.T., *et al.*, Self-propagating, molecular-level polymorphism in Alzheimer's β -amyloid fibrils. *Science* **307**, 262-265 (2005).
 20. Tycko, R., Amyloid polymorphism: Structural basis and neurobiological relevance. *Neuron* **86**, 632-645 (2015).
 21. Lu, J.X., *et al.*, Molecular structure of β -amyloid fibrils in Alzheimer's disease brain tissue. *Cell* **154**, 1257-1268 (2013).
 22. Qiang, W., Yau, W.M., Lu, J.X., Collinge, J., and Tycko, R., Structural variation in amyloid-

- β fibrils from Alzheimer's disease clinical subtypes. *Nature* **541**, 217-221 (2017).
23. Kollmer, M., *et al.*, Cryo-EM structure and polymorphism of A β amyloid fibrils purified from Alzheimer's brain tissue. *Nat. Commun.* **10**, 4760 (2019).
 24. Ghosh, U., Thurber, K.R., Yau, W.M., and Tycko, R., Molecular structure of a prevalent amyloid- β fibril polymorph from Alzheimer's disease brain tissue. *Proc. Natl. Acad. Sci. U. S. A.* **118**, (2021).
 25. Xiao, Y.L., *et al.*, A β (1-42) fibril structure illuminates self-recognition and replication of amyloid in Alzheimer's disease. *Nat. Struct. Mol. Biol.* **22**, 499-505 (2015).
 26. Walti, M.A., *et al.*, Atomic-resolution structure of a disease-relevant A β (1-42) amyloid fibril. *Proc. Natl. Acad. Sci. U. S. A.* **113**, E4976-E4984 (2016).
 27. Gremer, L., *et al.*, Fibril structure of amyloid- β (1-42) by cryo-electron microscopy. *Science* **358**, 116-119 (2017).
 28. Wang, H.S., *et al.*, Polymorphic A β 42 fibrils adopt similar secondary structure but differ in cross-strand side chain stacking interactions within the same β -sheet. *Sci Rep* **10**, (2020).
 29. Colvin, M.T., *et al.*, Atomic resolution structure of monomorphic A β (42) amyloid fibrils. *J. Am. Chem. Soc.* **138**, 9663-9674 (2016).
 30. Collinge, J., Mammalian prions and their wider relevance in neurodegenerative diseases. *Nature* **539**, 217-226 (2016).
 31. Caughey, B., Raymond, G.J., and Bessen, R.A., Strain-dependent differences in β -sheet conformations of abnormal prion protein. *J. Biol. Chem.* **273**, 32230-32235 (1998).
 32. Safar, J., *et al.*, Eight prion strains have PrP^{Sc} molecules with different conformations. *Nat. Med.* **4**, 1157-1165 (1998).
 33. Sanders, D.W., *et al.*, Distinct tau prion strains propagate in cells and mice and define different tauopathies. *Neuron* **82**, 1271-1288 (2014).
 34. Falcon, B., *et al.*, Structures of filaments from Pick's disease reveal a novel tau protein fold. *Nature* **561**, 137-140 (2018).
 35. Falcon, B., *et al.*, Novel tau filament fold in chronic traumatic encephalopathy encloses hydrophobic molecules. *Nature* **568**, 420-423 (2019).
 36. Fitzpatrick, A.W.P., *et al.*, Cryo-EM structures of tau filaments from Alzheimer's disease. *Nature* **547**, 185-190 (2017).

37. Zhang, W.J., *et al.*, Novel tau filament fold in corticobasal degeneration. *Nature* **580**, 283-287 (2020).
38. Tuttle, M.D., *et al.*, Solid state NMR structure of a pathogenic fibril of full-length human α -synuclein. *Nat. Struct. Mol. Biol.* **23**, 409-415 (2016).
39. Li, B.S., *et al.*, Cryo-EM of full-length α -synuclein reveals fibril polymorphs with a common structural kernel. *Nat. Commun.* **9**, (2018).
40. Schweighauser, M., *et al.*, Structures of α -synuclein filaments from multiple system atrophy. *Nature* **585**, 464-469 (2020).
41. Guo, J.L., *et al.*, Distinct α -synuclein strains differentially promote tau inclusions in neurons. *Cell* **154**, 103-117 (2013).
42. Bousset, L., *et al.*, Structural and functional characterization of two α -synuclein strains. *Nat. Commun.* **4**, (2013).
43. Woerman, A.L., *et al.*, Familial Parkinson's point mutation abolishes multiple system atrophy prion replication. *Proc. Natl. Acad. Sci. U. S. A.* **115**, 409-414 (2018).
44. Meyer-Luehmann, M., *et al.*, Exogenous induction of cerebral β -amyloidogenesis is governed by agent and host. *Science* **313**, 1781-1784 (2006).
45. Watts, J.C., *et al.*, Serial propagation of distinct strains of A β prions from Alzheimer's disease patients. *Proc. Natl. Acad. Sci. U. S. A.* **111**, 10323-10328 (2014).
46. Stohr, J., *et al.*, Distinct synthetic A β prion strains producing different amyloid deposits in bigenic mice. *Proc. Natl. Acad. Sci. U. S. A.* **111**, 10329-10334 (2014).
47. Cohen, M., *et al.*, Distinct strains of A β prions implicated in rapidly progressive Alzheimer disease. *Prion* **9**, S76-S77 (2015).
48. Rasmussen, J., *et al.*, Amyloid polymorphisms constitute distinct clouds of conformational variants in different etiological subtypes of Alzheimer's disease. *Proc. Natl. Acad. Sci. U. S. A.* **114**, 13018-13023 (2017).
49. Condello, C., *et al.*, Structural heterogeneity and intersubject variability of A β in familial and sporadic Alzheimer's disease. *Proc. Natl. Acad. Sci. U. S. A.* **115**, E782-E791 (2018).
50. Murray, D.T., *et al.*, Structure of FUS protein fibrils and its relevance to self-assembly and phase separation of low-complexity domains. *Cell* **171**, 615-627 (2017).
51. Elkins, M.R., *et al.*, Structural polymorphism of Alzheimer's β -amyloid fibrils as controlled

- by an E22 switch: A solid state NMR study. *J. Am. Chem. Soc.* **138**, 9840-9852 (2016).
52. Paravastu, A.K., Qahwash, I., Leapman, R.D., Meredith, S.C., and Tycko, R., Seeded growth of β -amyloid fibrils from Alzheimer's brain-derived fibrils produces a distinct fibril structure. *Proc. Natl. Acad. Sci. U. S. A.* **106**, 7443-7448 (2009).
53. Ghosh, U., Yau, W.M., and Tycko, R., Coexisting order and disorder within a common 40-residue amyloid- β fibril structure in Alzheimer's disease brain tissue. *Chem. Commun.* **54**, 5070-5073 (2018).
54. Kloepper, K.D., Woods, W.S., Winter, K.A., George, J.M., and Rienstra, C.M., Preparation of α -synuclein fibrils for solid state NMR: Expression, purification, and incubation of wild-type and mutant forms. *Protein Expr. Purif.* **48**, 112-117 (2006).
55. Luca, S., Yau, W.M., Leapman, R., and Tycko, R., Peptide conformation and supramolecular organization in amylin fibrils: Constraints from solid state NMR. *Biochemistry* **46**, 13505-13522 (2007).
56. Bennett, D.A., *et al.*, Religious orders study and Rush memory and aging project. *J. Alzheimers Dis.* **64**, S161-S189 (2018).
57. Qiang, W., Yau, W.M., and Tycko, R., Structural evolution of Iowa mutant β -amyloid fibrils from polymorphic to homogeneous states under repeated seeded growth. *J. Am. Chem. Soc.* **133**, 4018-4029 (2011).
58. Wold, S., Esbensen, K., and Geladi, P., Principal component analysis. *Chemometrics Intell. Lab. Syst.* **2**, 37-52 (1987).
59. Henry, E.R. and Hofrichter, J., Singular value decomposition: Application to analysis of experimental data. *Method Enzymol.* **210**, 129-192 (1992).
60. Yau, W.M. and Tycko, R., Depletion of amyloid- β peptides from solution by sequestration within fibril-seeded hydrogels. *Prot. Sci.* **27**, 1218-1230 (2018).
61. Aisen, P.S., *et al.*, On the path to 2025: Understanding the Alzheimer's disease continuum. *Alzheimers Res. Ther.* **9**, (2017).
62. Barulli, D. and Stern, Y., Efficiency, capacity, compensation, maintenance, plasticity: Emerging concepts in cognitive reserve. *Trends Cogn. Sci.* **17**, 502-509 (2013).
63. Busche, M.A. and Hyman, B.T., Synergy between amyloid- β and tau in Alzheimer's disease. *Nat. Neurosci.* **23**, 1183-1193 (2020).

Table 1: Statistics for RMSD analyses. Kolmogorov-Smirnov (KS) tests used $\alpha = 0.05$. Wilcoxon-Mann-Whitney (WMW) p values are two-tail values. The Welch's t-test (WTT) degree of freedom is v . RMSD 1 and RMSD 2 values are mean values, with standard deviations in parentheses. Underlined entries indicate statistically significant differences between RMSD values for comparison 1 and RMSD values for comparison 2. Italicized entries indicate an absence of statistical significance.

data type	comparison 1	RMSD 1	comparison 2	RMSD 2	KS D statistic	KS critical value	WMW U statistic	WMW p value	WTT v	WTT t statistic	WTT p value
2D ¹³ C- ¹³ C A β 40	RADC vs.RADC (n = 56)	0.246(0.104)	RADC vs. t-AD (n = 176)	0.311(0.065)	<u>0.312</u>	<u>0.222</u>	<u>3224.5</u>	<u><0.001</u>	<u>69.10</u>	<u>-4.322</u>	<u><0.001</u>
	RADC vs. RADC (n = 56)	0.246(0.104)	RADC vs. PCA (n = 144)	0.359(0.104)	<u>0.456</u>	<u>0.228</u>	<u>1811.5</u>	<u><0.001</u>	<u>90.19</u>	<u>-7.032</u>	<u><0.001</u>
	RADC vs. RADC (n = 56)	0.246(0.104)	RADC vs. t-AD+PCA-AD (n = 320)	0.332(0.082)	<u>0.357</u>	<u>0.210</u>	<u>5036</u>	<u><0.001</u>	<u>67.34</u>	<u>-5.827</u>	<u><0.001</u>
2D ¹⁵ N- ¹³ C A β 40	RADC vs.RADC (n = 56)	0.263(0.079)	RADC vs. t-AD (n = 176)	0.354(0.088)	<u>0.537</u>	<u>0.222</u>	<u>2113</u>	<u><0.001</u>	<u>101.17</u>	<u>-7.197</u>	<u><0.001</u>
	RADC vs. RADC (n = 56)	0.263(0.079)	RADC vs. PCA-AD (n = 96)	0.302(0.079)	<u>0.359</u>	<u>0.243</u>	<u>1748</u>	<u><0.001</u>	<u>90.08</u>	<u>-3.133</u>	<u>0.002</u>
	RADC vs. RADC (n = 56)	0.263(0.079)	RADC vs. t-AD+PCA-AD (n = 272)	0.336(0.083)	<u>0.473</u>	<u>0.213</u>	<u>3861</u>	<u><0.001</u>	<u>81.24</u>	<u>-6.112</u>	<u><0.001</u>
2D ¹³ C- ¹³ C A β 42	RADC vs.RADC (n = 42)	0.378(0.196)	RADC vs. t-AD (n = 98)	0.549(0.146)	<u>0.388</u>	<u>0.266</u>	<u>1235.5</u>	<u><0.001</u>	<u>59.39</u>	<u>-3.792</u>	<u><0.001</u>
	RADC vs. RADC (n = 42)	0.378(0.196)	RADC vs. PCA-AD (n = 98)	0.483(0.123)	<u>0.218</u>	<u>0.266</u>	<u>1731</u>	<u>0.137</u>	<u>58.63</u>	<u>-1.50</u>	<u>0.139</u>
	RADC vs. RADC (n = 42)	0.378(0.196)	RADC vs. t-AD+PCA-AD (n = 196)	0.516(0.147)	<u>0.260</u>	<u>0.246</u>	<u>2966.5</u>	<u>0.004</u>	<u>50.67</u>	<u>-2.761</u>	<u>0.008</u>
2D ¹⁵ N- ¹³ C A β 42	RADC vs.RADC (n = 42)	0.339(0.159)	RADC vs. t-AD (n = 98)	0.487(0.147)	<u>0.340</u>	<u>0.266</u>	<u>1248.5</u>	<u><0.001</u>	<u>75.41</u>	<u>-3.888</u>	<u><0.001</u>
	RADC vs. RADC (n = 42)	0.339(0.159)	RADC vs. PCA-AD (n = 56)	0.435(0.126)	<u>0.202</u>	<u>0.294</u>	<u>981</u>	<u>0.162</u>	<u>84.79</u>	<u>-1.558</u>	<u>0.122</u>
	RADC vs. RADC (n = 42)	0.339(0.159)	RADC vs. t-AD+PCA-AD (n = 154)	0.468(0.146)	<u>0.260</u>	<u>0.252</u>	<u>2229.5</u>	<u>0.002</u>	<u>63.65</u>	<u>-3.262</u>	<u>0.002</u>

Table 2: Statistics for principal component analyses. Results from WMW, KS, and WTT tests in t-AD, PCA-AD, and t-AD+PCA-AD rows represent comparisons with principal component coefficients of RADC data.

data type	principal component	tissue category	n	average coefficient	KS D statistic	KS critical value	WMW U statistic	WMW p value	WTT v	WTT t statistic	WTT p value
2D ¹³ C- ¹³ C Aβ40	1	RADC	8	0.192(0.031)							
	1	t-AD	11	0.182(0.035)	0.318	0.637	53	0.467	16.09	0.623	0.542
	1	PCA-AD	9	0.184(0.042)	0.222	0.663	37	0.925	14.61	0.435	0.670
	1	t-AD+PCA-AD	20	0.183(0.037)	0.200	0.579	90	0.618	15.29	0.630	0.538
	2	RADC	8	-0.225(0.197)							
	2	t-AD	11	0.061(0.094)	0.750	0.637	11	0.004	9.34	-3.804	0.004
	2	PCA-AD	9	0.131(0.071)	0.875	0.663	4	0.001	8.613	-4.843	0.001
	2	t-AD+PCA-AD	20	0.093(0.090)	0.750	0.579	15	<0.001	8.193	-4.383	0.002
	3	RADC	8	-0.086(0.263)							
	3	t-AD	11	0.036(0.148)	0.409	0.637	34	0.418	10.217	-1.183	0.264
	3	PCA-AD	9	0.082(0.143)	0.500	0.663	16	0.053	10.539	-1.607	0.138
	3	t-AD+PCA-AD	20	0.057(0.144)	0.45	0.579	50	0.129	8.732	-1.450	0.182
2D ¹⁵ N- ¹³ C Aβ40	1	RADC	8	0.197(0.023)							
	1	t-AD	11	0.198(0.029)	0.284	0.637	43	0.936	16.909	-0.104	0.918
	1	PCA-AD	6	0.199(0.038)	0.333	0.729	21	0.708	7.621	-0.115	0.911
	1	t-AD+PCA-AD	17	0.199(0.031)	0.199	0.592	64	0.820	18.784	-0.137	0.893
	2	RADC	8	-0.134(0.198)							
	2	t-AD	11	0.093(0.201)	0.568	0.637	18	0.029	15.374	-2.467	0.026
	2	PCA-AD	6	0.070(0.102)	0.625	0.729	10	0.070	10.911	-2.516	0.029
	2	t-AD+PCA-AD	17	0.085(0.169)	0.574	0.592	28	0.017	12.013	-2.712	0.019
	3	RADC	8	-0.092(0.173)							
	3	t-AD	11	0.030(0.246)	0.364	0.637	28	0.191	16.996	-1.275	0.219
	3	PCA-AD	6	0.028(0.144)	0.458	0.729	15	0.255	11.812	-1.427	0.180
	3	t-AD+PCA-AD	17	0.030(0.210)	0.390	0.592	43	0.148	16.617	-1.531	0.144
2D ¹³ C- ¹³ C Aβ42	1	RADC	8	-0.233(0.023)							
	1	t-AD	7	-0.193(0.021)	0.857	0.702	5	0.005	12.947	-3.511	0.004
	1	PCA-AD	7	-0.204(0.025)	0.607	0.702	10	0.034	12.229	-2.296	0.040
	1	t-AD+PCA-AD	14	-0.199(0.023)	0.714	0.610	15	0.003	14.881	-3.374	0.004
	2	RADC	8	0.186(0.130)							
	2	t-AD	7	-0.197(0.205)	0.875	0.702	54	0.001	9.933	4.255	0.002
	2	PCA-AD	7	-0.044(0.106)	0.875	0.702	51	0.005	12.951	3.766	0.002
	2	t-AD+PCA-AD	14	-0.121(0.176)	0.875	0.610	105	<0.001	18.408	4.661	<0.001
	3	RADC	8	-0.075(0.326)							
	3	t-AD	7	-0.007(0.113)	0.375	0.702	27	0.911	8.843	-0.547	0.598
	3	PCA-AD	7	0.107(0.095)	0.500	0.702	19	0.308	8.334	-1.505	0.169
	3	t-AD+PCA-AD	14	-0.050(0.116)	0.375	0.610	46	0.504	8.033	-1.043	0.328
2D ¹⁵ N- ¹³ C Aβ42	1	RADC	8	-0.220(0.017)							
	1	t-AD	7	-0.241(0.037)	0.589	0.702	39	0.210	8.241	1.333	0.218
	1	PCA-AD	4	-0.220(0.028)	0.375	0.813	17	0.871	4.185	-0.039	0.970
	1	t-AD+PCA-AD	11	-0.233(0.034)	0.420	0.637	56	0.330	15.512	1.063	0.304
	2	RADC	8	0.197(0.067)							
	2	t-AD	7	-0.185(0.229)	1.000	0.702	56	<0.001	6.897	4.263	0.004
	2	PCA-AD	4	0.030(0.180)	0.750	0.813	27	0.060	3.423	1.801	0.158
	2	t-AD+PCA-AD	11	-0.107(0.230)	0.909	0.637	83	<0.001	12.225	4.151	0.001
	3	RADC	8	-0.070(0.358)							
	3	t-AD	7	0.047(0.031)	0.625	0.702	19	0.308	7.121	-0.918	0.389
	3	PCA-AD	4	0.100(0.027)	0.750	0.831	8	0.183	7.157	-1.328	0.225
	3	t-AD+PCA-AD	11	0.066(0.039)	0.625	0.637	27	0.164	7.119	-1.068	0.321

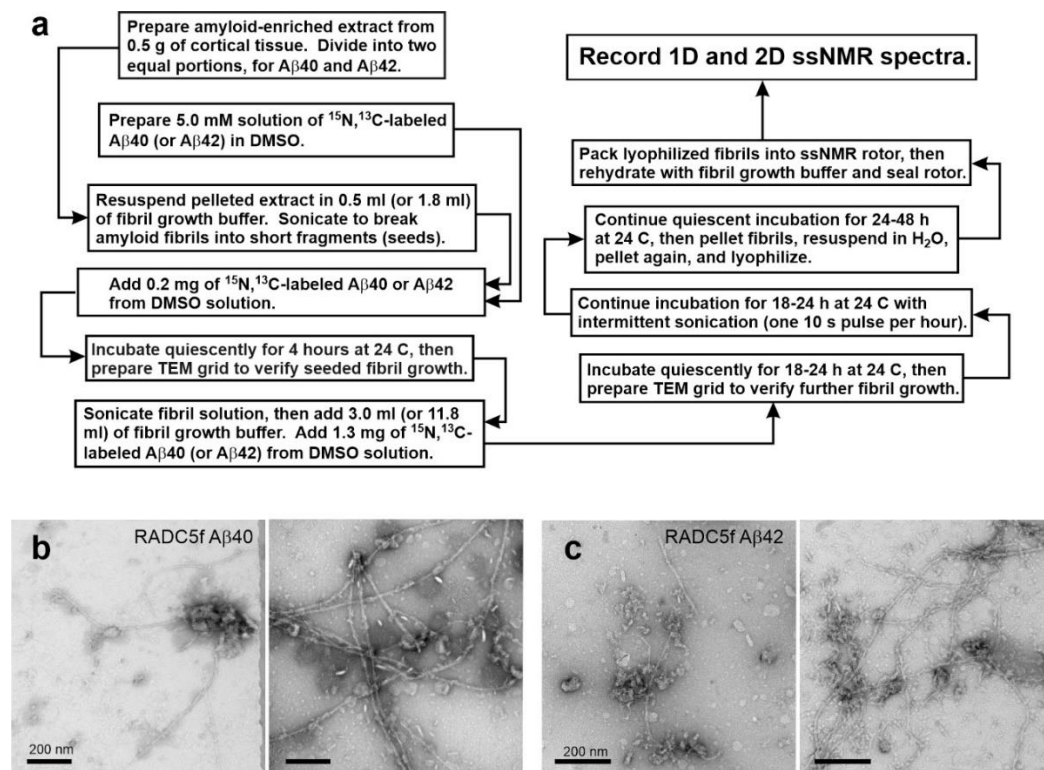


Figure 1: Preparation of brain-seeded A β fibrils for solid state NMR. (a) Flowchart representation of the protocol for preparation of isotopically labeled A β 40 and A β 42 fibril samples by seeded growth from amyloid in human brain extract. (b) TEM images of negatively stained A β 40 fibrils prepared from frontal lobe tissue of RADC subject 5. Images are shown after the initial 4 h incubation step (left) and after the subsequent 18-24 h incubation step (right). (c) Same as panel a, but for A β 42 fibrils. All scale bars are 200 nm.

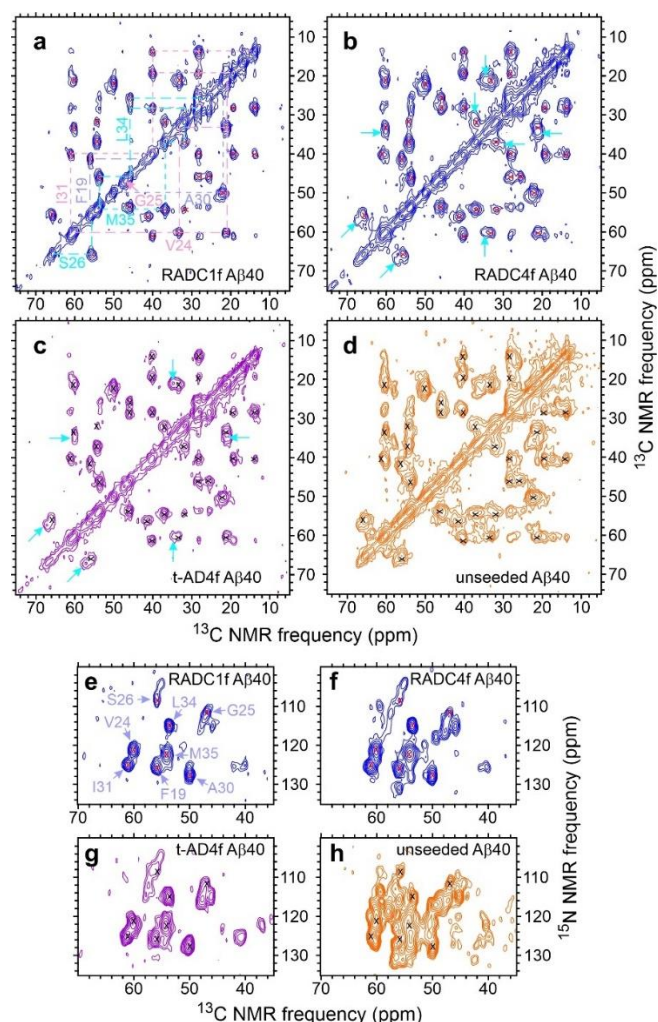


Figure 2: 2D solid state NMR spectra of brain-seeded A β 40 fibrils with uniform ^{15}N , ^{13}C -labeling of F19, V24, G25, S26, A30, I31, L34, and M35. (a-d) 2D ^{13}C - ^{13}C spectra of fibrils prepared from frontal lobe tissue of RADC subjects 1 and 4, fibrils prepared from frontal lobe tissue of AD patient t-AD4 (as reported previously by Qiang *et al.* (22)), and unseeded fibrils. Assignments of crosspeak signals to the labeled residues are indicated by cyan, pink, and pastel blue labels and dashed lines in panel a. Red or black X's in panels b-d indicate positions of crosspeak signals in panel a. Cyan arrows indicate additional crosspeak signals. Contour levels increase by successive factors of 2.0, with the lowest contour at approximately 3.0 times the root-mean-squared (rms) noise level in each spectrum. (e-f) 2D ^{15}N - ^{13}C spectra of the same fibrils, with similar annotations. Contour levels increase by successive factors of 1.5, with the lowest contour at approximately 3.0 times the rms noise level. The full set of 2D spectra of A β 40 fibrils prepared from RADC samples is given in the SI Appendix, Figs. S4 and S5.

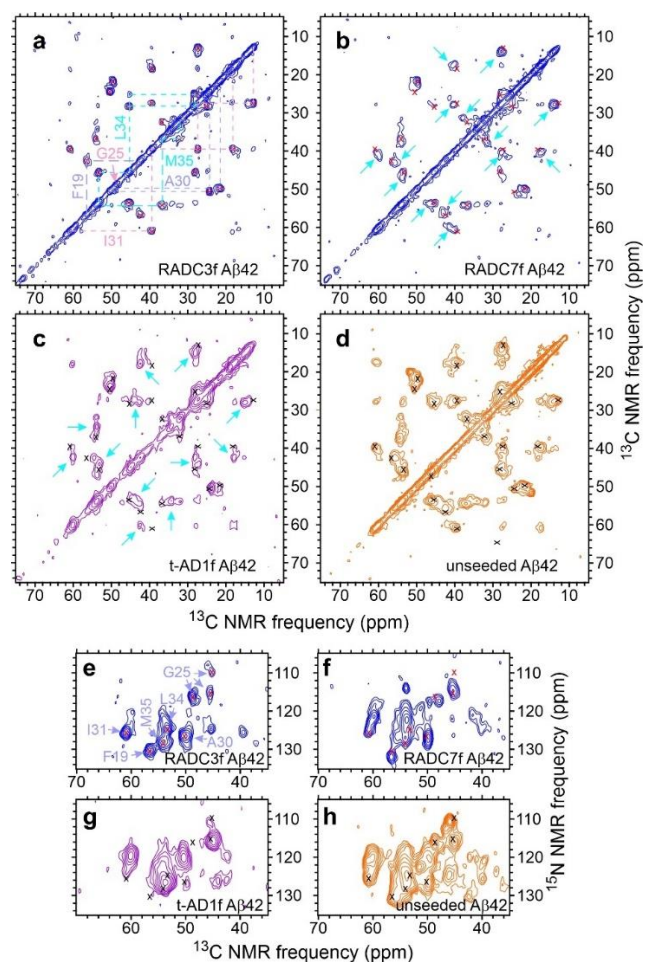


Figure 3: 2D solid state NMR spectra of brain-seeded A β 42 fibrils with uniform ^{15}N , ^{13}C -labeling of F19, G25, A30, I31, L34, and M35. (a-d) 2D ^{13}C - ^{13}C spectra of fibrils prepared from frontal lobe tissue of RADC subjects 3 and 7, fibrils prepared from frontal lobe tissue of AD patient t-AD1 (as reported previously by Qiang *et al.* (22)), and unseeded fibrils. Assignments of crosspeak signals to the labeled residues are indicated by cyan, pink, and pastel blue labels and dashed lines in panel a. Red or black X's in panels b-d indicate positions of crosspeak signals in panel a. Cyan arrows indicate additional crosspeak signals. Contour levels increase by successive factors of 2.0, with the lowest contour at approximately 3.0 times the root-mean-squared (rms) noise level in each spectrum. (e-h) 2D ^{15}N - ^{13}C spectra of the same fibrils, with similar annotations. Contour levels increase by successive factors of 1.5, with the lowest contour at approximately 3.0 times the rms noise level. The full set of 2D spectra of A β 42 fibrils prepared from RADC samples is given in the SI Appendix, Figs. S6 and S7.

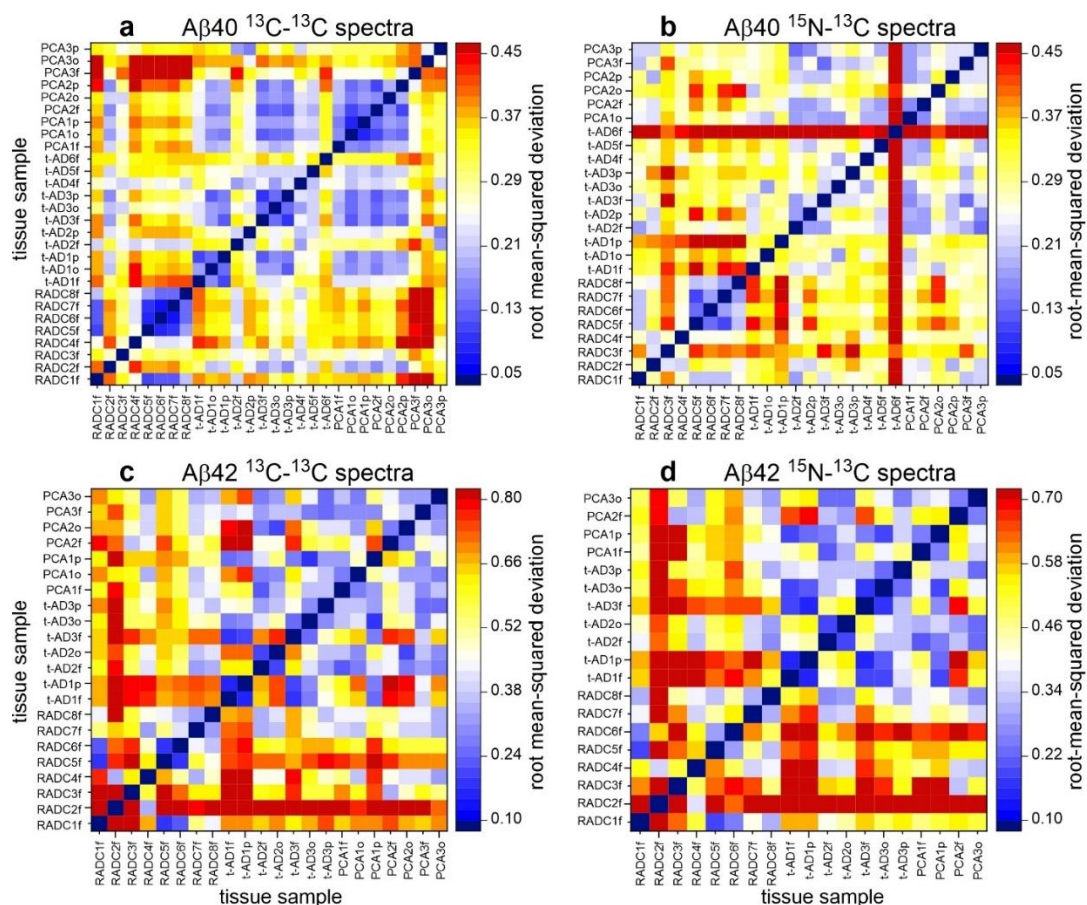


Figure 4: Comparisons of 2D solid state NMR spectra of isotopically labeled A β 40 and A β 42 fibrils derived from cortical tissue of non-demented subjects (RADCn f , where n is the patient number), typical Alzheimer's disease patients (t-ADn x , where x is f , o , or p for frontal, occipital, or parietal lobe tissue), and posterior cortical atrophy patients (PCAn x). Color scales represent root-mean-squared differences (RMSDs) between crosspeak signal amplitudes in pairs of 2D spectra, after normalization and optimal scaling of the 2D spectra as described in the text. (a,b) RMSD heat maps for 2D ^{13}C - ^{13}C and ^{15}N - ^{13}C spectra of A β 40 fibrils. (c,d) RMSD heat maps for 2D ^{13}C - ^{13}C and ^{15}N - ^{13}C spectra of A β 42 fibrils.

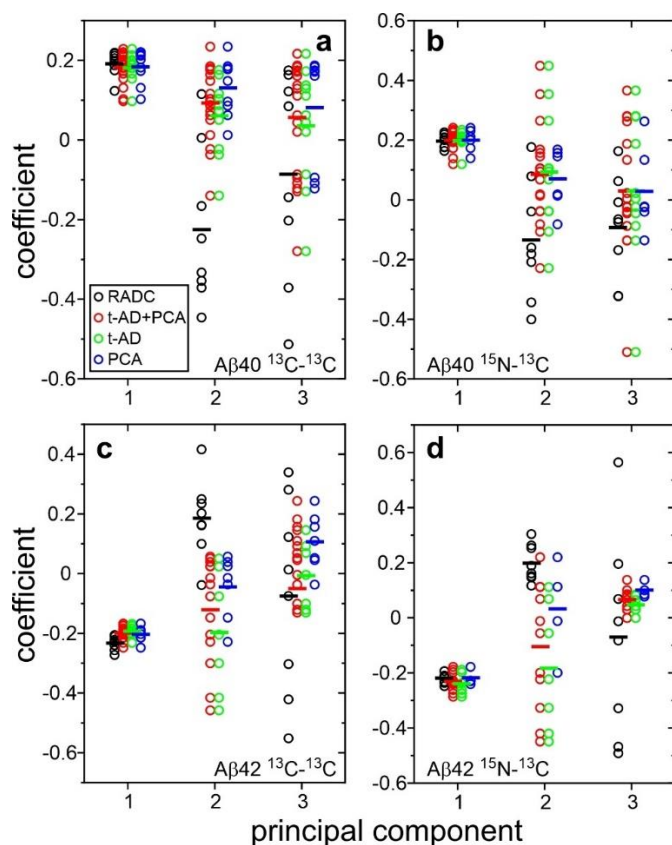


Figure 5: Comparisons of 2D solid state NMR spectra of isotopically labeled A β 40 and A β 42 fibrils by principal component analysis. (a) Coefficients of the first three principal components in 2D ^{13}C - ^{13}C spectra of A β 40 fibrils derived from RAD, t-AD, and PCA-AD tissue samples. Color-coded circles indicate coefficients for individual 2D spectra. Bars indicate average values. Combined data for t-AD and PCA samples are shown as "t-AD+PCA". (b) Same as panel a, for 2D ^{15}N - ^{13}C spectra. (c,d) Same as panels a and b, but for A β 42 fibrils.

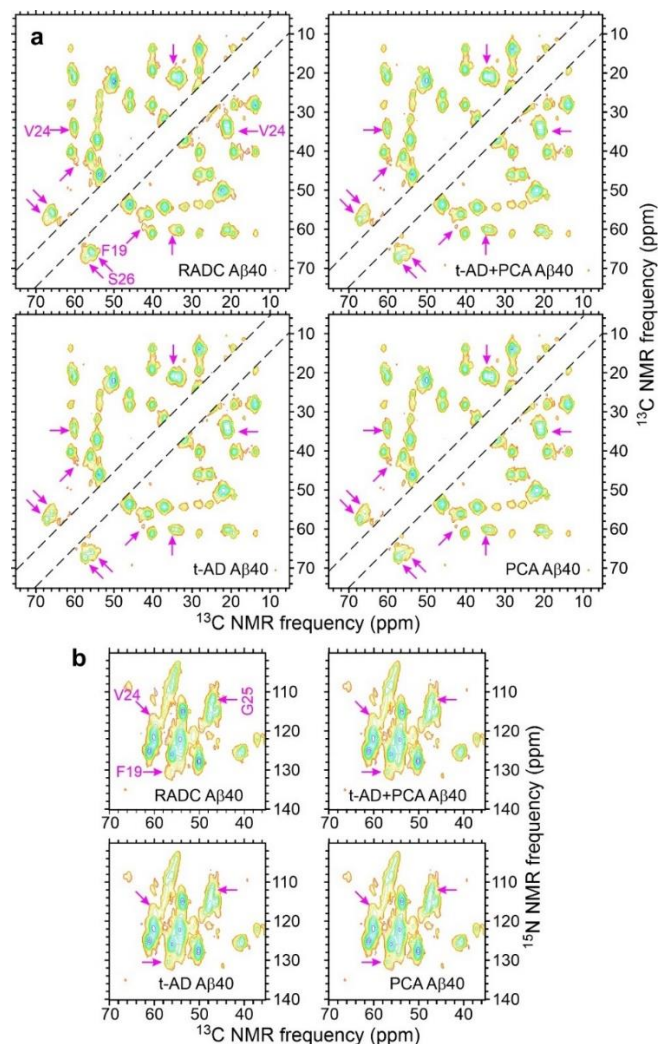


Figure 6: Average 2D spectra generated from principal component spectra, using the average coefficients of the first three principal components in each tissue category. (a) Average 2D ^{13}C - ^{13}C spectra of isotopically labeled A β 40 fibrils derived from RADC, t-AD, and PCA-AD tissue samples. Combined averages for t-AD and PCA-AD samples are shown as "t-AD+PCA". Sixteen contour levels are shown, increasing by factors of 1.4 and with colors ranging from red to blue. Diagonal regions within dashed lines were not included in the principal component analysis. Magenta arrows indicate crosspeaks with subtle variations in relative intensities. (b) Same as panel a, for 2D ^{15}N - ^{13}C spectra. The numbers of spectra used to calculate averages for RADC, t-AD+PCA, t-AD, and PCA categories are 8, 20, 11, and 9 in panel a and 8, 17, 11, and 6 in panel b.

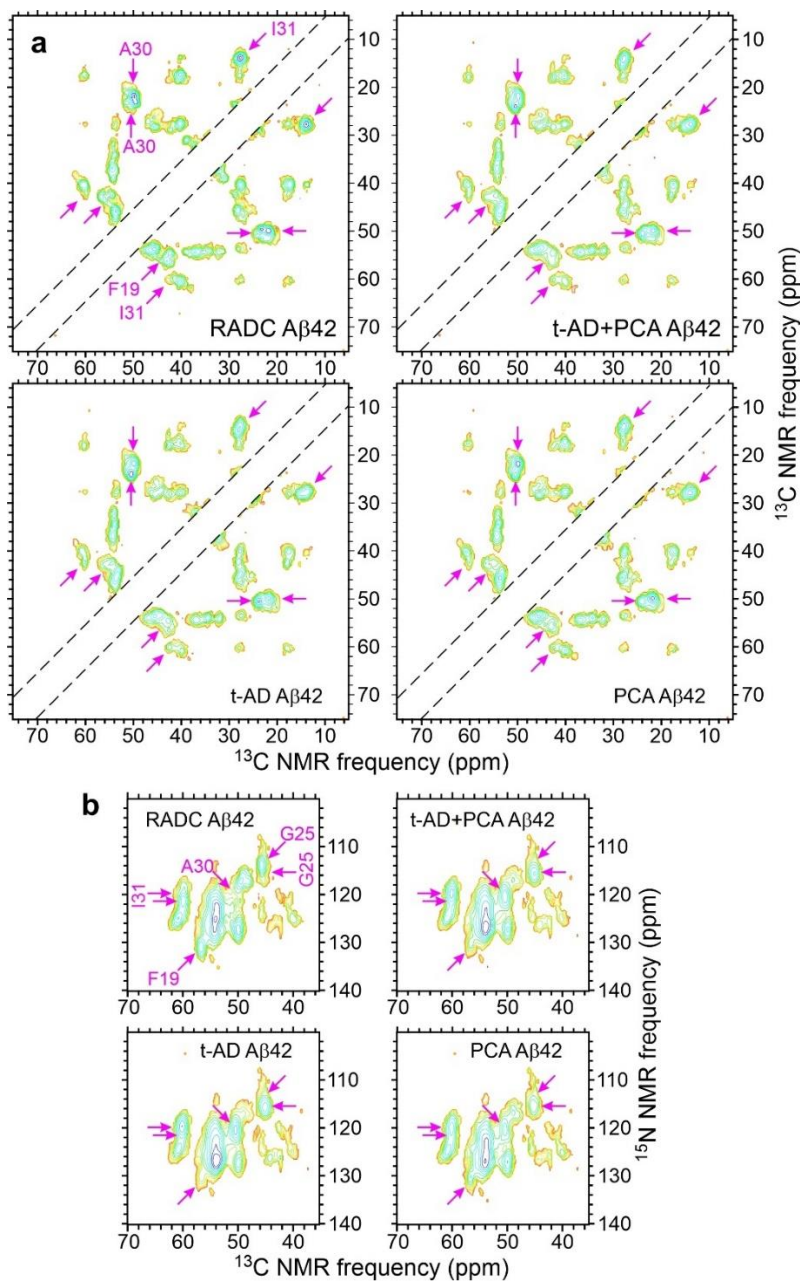


Figure 7: Average 2D spectra of isotopically labeled A β 42 fibrils, as in Fig. 6. The numbers of spectra used to calculate averages for RADC, t-AD+PCA, t-AD, and PCA categories are 8, 14, 7, and 7 in panel a and 8, 11, 7, and 4 in panel b.